Fizika Nizkikh Temperatur, 2009, v. 35, No. 1, p. 116–121

Statistical model structure of $A_{1-x}Z_xB_2$ Laves phase C15 system — the superconducting $Ce_{1-x}La_xRu_2$ alloy

B.V. Robouch and A. Marcelli

Istituto Nazionale di Fisica Nucleare, Laboratori Nazionali di Frascati, Via Enrico Fermi 40, I-00044 Frascati, Italy
E-mails: robouch@lnf.infn.it

N.L. Saini

Dipartimento di Fisica, Universitá di Roma «La Sapienza» P. le Aldo Moro 2, 00185 Roma, Italy

A. Kisiel

Instytut Fizyki, Universytet Jagiellonski, Reymonta 4, 30-059 Krakow, Poland

Received July 8, 2008

Local structure of $Ce_{1-x}La_xRu_2$ system, measured by EXAFS has been re-examined and correlated to the statistical ad hoc model, recently applied to the sphalerite, wurtzite and other intermetallic ternary alloys. The deconvolution of the EXAFS data show that the $Ce_{1-x}La_xRu_2$ ternary system is essentially a mixture of: $CeRu_2$ and $LaRu_2$ binary alloys with a small proportion of the $Ce_{0.5}La_{0.5}Ru_2$ ternary configuration, being maximum for the intermediate concentration. Moreover, the analysis reveals that while the $LaRu_2$ configuration exhibits a Bernoulli random distribution, the presence of a Ce atom affects both the $CeRu_2$ and $Ce_{0.5}La_{0.5}Ru_2$ distributions, strongly favoring the configuration with the CeCe pair, while keeping rare that with a single Ce ion.

PACS: *61.05.cj* X-ray absorption spectroscopy: EXAFS, NEXAFS, XANES;
74.70.Ad Metals; alloys and binary compounds (including A15, MgB_2, etc.);
74.70.Tx Heavy-fermion superconductors.

Keywords: Laves phases, $Ce_{1-x}La_xRu_2$ system, local structure, statistical model.

1. Introduction

The Laves phases are generally found in the AB_2 composition. The peculiarity of this structure is that B atoms are assembled in tetrahedra around the A atoms, while atoms A are ordered in: 1) a cubic $MgCu_2$ type C15 structure (e.g., $CsBi_2$, $RbBi_2$, $TbFe_2$, $DyFe_2$, FePd), 2) a hexagonal $CaMg_2$ type C14 structure (e.g., $ZrRe_2$, KNa_2, $TaFe_2$, $NbMn_2$, UNi_2, $TiMn_2$) or 3) an $NbZn_2$ type C36 structure (e.g., $ScFe_2$, $ThMg_2$, $HfCr_2$, UPt_2). Several other crystalline systems such as $AuBe_5$, $AuNi_4Y$, Pt_5U, etc. also have a Laves cubic $C15_b$ structure, while other AB_2 crystals (e.g., MgB_2) grow with non-Laves structures in which the B atoms form graphite like sheets separated by hexagonal Mg layers. Many compounds crystallizing in the AB_2 structures have been investigated, such as UGe_2 [1], MgB_2 [2,3], $ZrZn_2$ [4], $CaSi_2$ [5,6], RFe_2 (R = rare earths) [7], or ternary $NbCr_2$ loaded with Ti, V, Zr, Mo, W [8].

$CeRu_2$ is one of the most interesting Laves phase alloys, partly due to its unusual superconducting and magnetic properties [9]. $CeRu_2$ exhibits superconductivity at 6.2 K [10–17] but also $LaRu_2$ is a superconductor with $T_c \sim 4$ K; although the two compounds are probably associated to different superconductivity mechanisms. Here we focus on the $Ce_{1-x}La_xRu_2$ ternary system, an $MgCu_2$ type C15 Laves crystal, to understand its functional behavior and to further characterize its local structure [17].

2. Topology of $MgCu_2$ type C15 crystals: $CeRu_2$ and $LaRu_2$

The Laves $MgCu_2$ type cubic C15 structured phases are identified by the *cF*24 Pearson symbol, space group *Fd*3m, and number 227 [18]. The crystal lattice structure is defined by its:

– primitive vectors: $\{j\,a/2 + k\,a/2,\ i\,a/2 + k\,a/2,\ i\,a/2 + j\,a/2\}$, (1)

and

– basic vectors:
$$B_{Mg1} = i\,a/8 + j\,a/8 + k\,a/8; \quad B_{Mg2} = i\,7a/8 + j\,7a/8 + k\,7a/8;$$
$$B_{Cu1} = i\,a/2 + j\,a/2 + k\,a/2; \quad B_{Cu2} = i\,a/2 + j\,a/4 + k\,a/4;$$
$$B_{Cu3} = i\,a/4 + j\,a/2 + k\,a/4; \quad B_{Cu4} = i\,a/4 + j\,a/4 + k\,a/2 \quad (2)$$

[18]* (see Figs. 1 and 2).

$CeRu_2$ and $LaRu_2$ are binary systems canonically characterized by the $MgCu_2$ structure (Fig. 1) and described by Wyckoff [18] with Eqs. (1) and (2); all interatomic distances are given in Table 1 [19,20]. Thus in the binary Ce_2Ru_4, the Ru-vertex is midway between the two Ce atoms.

However, Huxley et al. [12] reported that their unannealed $CeRu_2$ *twinned* crystals differ slightly from the ideal $MgCu_2$ structure, and suggest the less symmetric phase characterized by $F43m$ space group structure instead of the normal $Fd3m$ (Fig. 2).

3. The ternary $(Ce_{1-x}La_x)_2Ru_4$ model structure

The ternary $(Ce_{1-x}La_x)_2Ru_4$ structure has three possible configurations (T_0,T_1,T_2) where a subscript index indicates the number of La atoms substituted for the Ce in the Ce_2Ru_4 binary. For example, the T_0 is a binary Ce_2Ru_4, T_1 is a ternary $CeLaRu_4$ and T_2 is a binary La_2Ru_4. Site occupation preferences (SOPs) are possible in the T_1 configuration only, with the weight coefficient W_1 quantifying the departure from a random distribution [21].

For a random distribution of Ce and La atoms with respective relative contents $(1 - x)$ and x in the sample, the probability of occupation in the three configurations is described by Bernoulli's binomials

$$p^{[N]}_k = !N/[!k\,!(N-k)]\,x^k(1-x)^{N-k} \quad (3)$$
$$\text{with } \Sigma_{k=0,N}\,[p^{[N]}_k] \equiv 1,$$

where N is the number of available sites to be filled, k is the number of La atoms and $(N - k)$ that of Ce atoms in the resulting configuration [22]. In $CeLaRu_4$, $N = 2$ and hence we write for the probabilities $p_k = p^{[2]}_k$:

$p_0 = (1-x)^2$, $p_1 = 2x(1-x)$, $p_2 = x^2$, with $0 \le W_1 \le 2$ [21].

In the Laves structure (Fig. 1) the Ce and La atoms are surrounded by Ru atoms and the coordination numbers (CN) for the NN and the NNN atoms are

$$^{NN}_{Ce}{}^{Ru}CN = {}^{NN}_{La}{}^{Ru}CN = 12,\ {}^{NN}_{Ru}{}^{Ru}CN = 6,$$
$$\text{and } {}^{NNN}_{Ru}{}^{Ce}CN = {}^{NNN}_{Ru}{}^{La}CN = 6,$$
$$\text{while } 0 \le {}^{NNN}_{Ce}{}^{Ce}CN = 4P_0 + 2P_1 \le 4$$
$$\text{and } 0 \le {}^{NNN}_{La}{}^{La}CN = 2P_1 + 4P_2 \le 4$$
$$\text{with } {}^{NNN}_{Ce}{}^{La}CN = 4 - {}^{NNN}_{Ce}{}^{Ce}CN \le 4,$$
$$\text{and } {}^{NNN}_{La}{}^{Ce}CN = 4 - {}^{NNN}_{La}{}^{La}CN \le 4 \text{ [19]}, \quad (4)$$

where

$$P_0 = p_0 + \max[0;(1 - W_1)]p_1;$$
$$P_1 = \min[W_1;\ 1;\ (2 - W_1)]p_1;$$
$$P_2 = p_2 + p_1\max[0;(1 - W_1)]$$

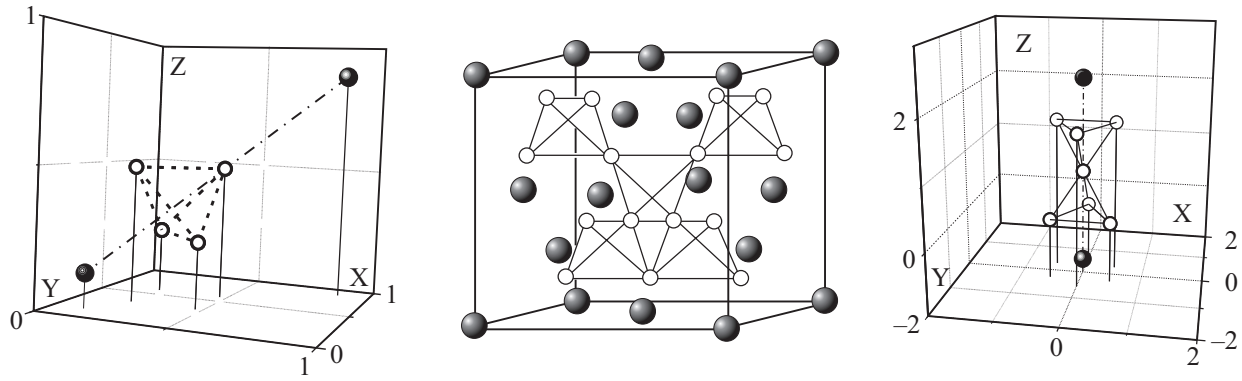

Fig. 1. (left) Perspective view of the atomic distribution in the Mg_2Cu_4 structural element: Mg (●), Cu (○), crystal axis (dash dot), Cu tetrahedron (short dash) as described in Ref. 18; (center) Basic structure unit cell of the $MgCu_2$ type C15 crystal. Mg (●), Cu (○); (right) Perspective view of the atomic distribution of a $CeRu_2$ crystal (as per [12]): Ce (●), Ru (○) forming the vertex sharing tetrahedra (dot), crystal axis (dash dot).

* Wyckoff [18] crystal structure nomenclature is adopted throughout the text.

Table 1. Crystal lattice parameter, near neighbours (NN) and next near neighbours (NNN) coordination numbers and the interatomic distances a for the $CeRu_2$ and $LaRu_2$ [19,20]

Binary	a, Å	NN					NNN					
		12	Ru:Ru	6	Ce:Ru	La:Ru	12	Ce:Ru	La:Ru	4	Ce:Ce	La:La
$CeRu_2$	7.537		2.665		3.125	–		3.125			3.264	
$LaRu_2$	7.718		2.729		–	3.200			3.200			3.342

conserving the stoichiometry [21]. The canonical structure and that proposed by Huxley et al. structures differ by distances and hence we need comparison of both structures.

3.1. Structural assumptions

Two occupation sites for the competing Ce and La atoms (indicated as spheres in the Fig. 1) are known. The binary configurations T_0 and T_2 are defined (Table 1), while the ternary T_1 requires to be modeled with one SOP coefficient W_1, and three inter-atomic distances ${}^{Ru}_{Ru}d_1$, ${}^{Ru}_{Ce}d_1$ ($\equiv {}^{Ce}_{Ru}d_1$), ${}^{Ru}_{La}d_1$ ($\equiv {}^{La}_{Ru}d_1$). The model also considers that in the ternary configuration T_1:

– each Ce and La atoms are centered within its NN first spherical shell of the surrounding Ru atoms, with the respective radii ${}^{Ru}_{Ce}d_1$ and ${}^{Ru}_{La}d_1$;

– the size of the Ru tetrahedra coordinated with Ce atoms is ${}_{Ce}{}^{RuRu}d_1$ while those coordinated with the La atoms is ${}_{La}{}^{RuRu}d_1$. The experimental data does not allow distinguishing between these two parameters and therefore they are assumed to be equal to the experimental values of the ${}^{Ru}_{Ru}d_1$.

The resulting crystal size should simulate the observed lattice constant in the ternary configuration T_1 (see Fig. 3).

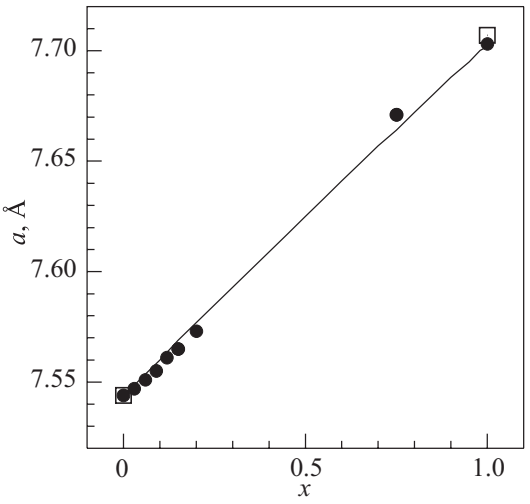

Fig. 2. The $Ce_{1-x}La_xRu_2$ lattice constant a vs. x: calculations (solid); experimental data (●), values of end members from literature [20] (□).

3.2. Resulting equations

Applying the probabilistic description of the EXAFS data of the atomic pairs, as it has been done previously for sphalerite, wurtzite and other intermetallides [21,23–25] we obtain, in agreement with the above assumptions, the following expressions:

$$<{}^{Ru}_{Ru}d> = 12\{{}^{Ru}_{Ru}d_0P_0 + {}^{Ru}_{Ru}d_1P_1 + {}^{Ru}_{Ru}d_2P_2\}/12,$$

$$<{}^{Ru}_{Ce}d> = \{12\,{}^{Ru}_{Ce}d_0P_0 + 6\,{}^{Ru}_{Ce}d_1P_1\}/[12P_0 + 6P_1],$$

$$<{}^{Ru}_{La}d> = \{6\,{}^{Ru}_{La}d_0P_1 + 12\,{}^{Ru}_{La}d_2P_2)\}/[6P_1 + 12P_2],$$

$$<a_{CeLaRu_2}> = \{a_{CeRu_2}P_0 + a_{CeLaRu_2}P_1 + a_{LaRu_2}P_2\}/1.$$

Thus according to the model we have four free parameters, the SOP coefficient W_1 and three distance parameters relative to the configuration T_1, to reproduce the experimental values of Fig. 2–4.

4. Experimental data

Ru K-edge x-ray absorption fine structure (EXAFS) spectroscopy, a fast and local tool capable to probe a small local cluster (~ 5–6 Å) around the photo absorber [26] was used to determine the local displacements in the $Ce_{1-x}La_xRu_2$ system. This system is indeed characterized by a short coherence length (~ 30–60 Å), and local interactions are expected to be important for its superconducting behavior. As diffraction does not show any structural anomaly as a function of the La concentration at ambient pressure [27], the EXAFS method was considered to explore possible structure-function relationship in this system.

4.1. Sample preparation and characterization

Samples of $Ce_{1-x}La_xRu_2$ (with x = 0, 0.03, 0.06, 0.09, 0.12, 0.15, 0.151, 0.20, 0.75, 0.751) were synthesized by arc melting [17]. All the samples were characterized by x-ray diffraction (Cu K_α source with Si standard) for their long range structural properties [9]. The diffraction data revealed $MgCu_2$-type structure with unavoidable impurities estimated at ≤ 2–3% (impurities probably contained in the starting metallic ingredients). For these samples, the measured lattice parameters a and the average interatomic distances Ru:Ru and Ru:Ce vs. x are summarized in Table 2.

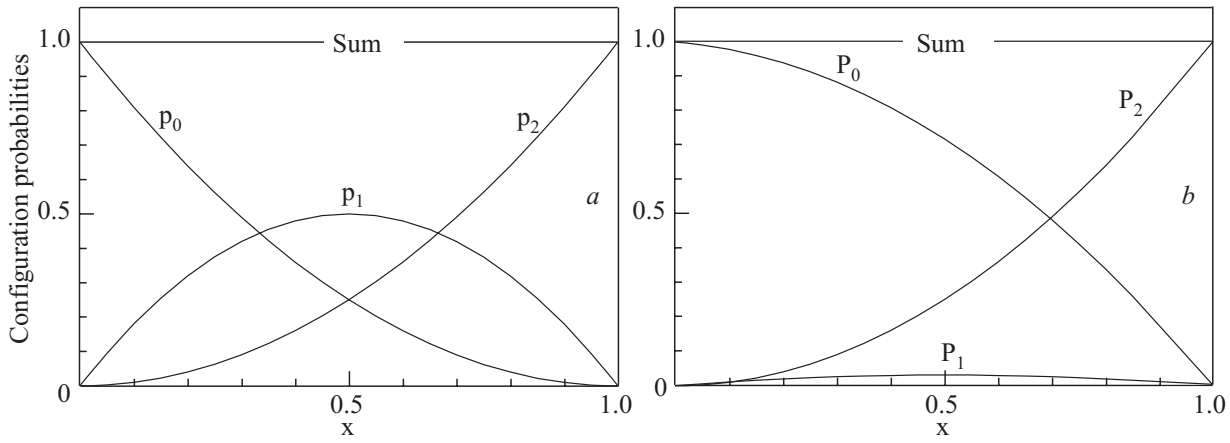

Fig. 3. Comparison of the random probabilities p_k's (panel *a*) of the three configurations T_0, T_1, T_2 and of their sum vs. x with P_k's (panel *b*), those achieved from experimental data.

4.2. EXAFS measurements

Ru *K*-edge absorption measurements were performed on powdered $Ce_{1-x}La_xRu_2$ samples. The EXAFS measurements were carried out in Grenoble at the beam line BM29 of the European Synchrotron Radiation Facility (ESRF) using radiation monochromatized with a double crystal Si(311) monochromator. Ru K_α fluorescence yield was collected using a multi-element Ge detector array. The samples were mounted in a closed cycle two stage He refrigerator to ensure measurements at $T = (30 \pm 1)$ K. Routinely, several absorption scans were collected to test the reproducibility of the spectra, and to limit the noise level to the order of 10^{-4} to achieve a high S/N ratio. the EXAFS signal was extracted from the absorption spectrum using the standard procedure [26], followed by the x-ray fluorescence self-absorption correction before the analysis [28]. The obtained results are summarized in Table 2 and plotted in Figs. 2 and 4.

5. Results

Regarding the T_1 configuration of the $CeLaRu_2$ system our calculations showed that $W_1 = 0.063 \pm 0.001$ (C_1= = 6.3% of a random distribution) with T_1 inter ion NN distances: Ce:Ru = 5.360 Å; Ru:Ru = 3.122 Å while La:Ru is poorly defined due to its low abundance.

With a unit cell parameter $a = 8.861$ Å, the above results imply:

– a strong preference for the Ce atoms with respect to La (see Fig. 3);

– an expanded T_1 configuration for the $Ce_{0.5}La_{0.5}Ru_2$, i.e., with a lattice constant ≈16% greater than the mean lattice of either of the two binary $CeRu_2$ or $LaRu_2$;

– an inter ion NN distance Ru:Ru ≈17% greater than the corresponding mean distance of the two binary $CeRu_2$ and $LaRu_2$;

– an inter ion NN distance Ce:Ru ≈ 73% greater than that of the binary $CeRu_2$.

In his work Huxley et al. [17] reported for their unannealed crystals twin structures (Fig. 1) a strongly distorted structure «with alternate Ru-tetrahedra enlarged (I) or compressed (II)» and also «two distinct environments, type Ce_I and Ce_{II}» for cerium atoms. At first sight, available experimental data do not support different structural configurations. In order to test the compatibility of the data with two distinct Ce environments and eventually the occurrence of different environments also for La, we estimated the experimental error bars. In the case of two families of distances (Ce_I and Ce_{II}) the uncertainties may be due both to experimental errors and to the different contributions. Thus to set a possible upper value to the distance variation between Ce_I and Ce_{II} environments, we assume the experimental error equal to zero, at-

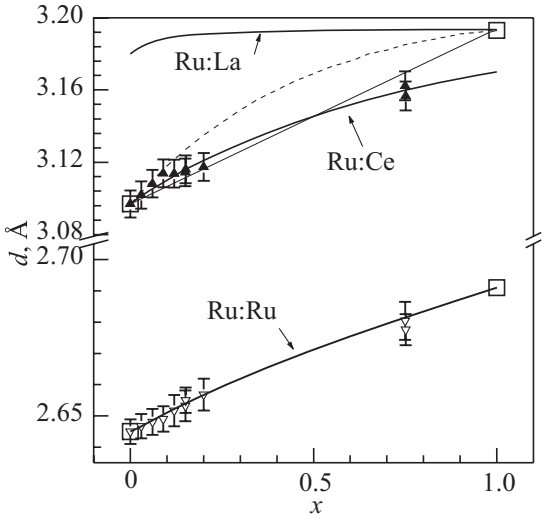

Fig. 4. $Ce_{1-x}La_xRu_2$ interatomic distances d vs. x: calculations and experimental data of Ru:Ru (▽), Ru:Ce (▲); Ru:La (curve) [17]. □ are values of end members from [20]. Vegard line (solid thin), VCA curve (dashed).

Table 2. Lattice parameter a and average interatomic Ru:Ru and Ru:Ce distances vs. x measured by Ru K-edge EXAFS. The average uncertainty for Ru–Ru distances is $\Delta_{RuRu} = \pm 0.006$ Å and for Ru–Ce is $\Delta_{RuCe} = \pm 0.01$ Å

$x =$	0	0.03	0.06	0.09	0.12	0.15	0.151	0.2	0.75	0.751	1
a [Å]	7.544	7.547	7.551	7.555	7.561	7.565	7.565	7.573	7.671	7.671	7.703
Ru:Ru [Å]	2.645	2.647	2.648	2.649	2.652	2.653	2.655	2.657	2.680	2.678	
Ru:Ce [Å]	3.097	3.102	3.108	3.114	3.114	3.114	3.116	3.117	3.162	3.157	

tributing the entire variation to the difference Δ of the two distances: ${}^{Ru}_{CeI}d_1$ and ${}^{Ru}_{CeII}d_1$. Thus the deconvolution would determine the ${}^{Ru}_{Ce}d_1$ = mean $({}^{Ru}_{CeI}d_1;\ {}^{Ru}_{CeII}d_1)$ with the error bar Δ_{CeRu} from Table 2: ${}^{Ru}_{Ce}d_1 = 3.097$ with $\Delta_{RuCe} = 0.01$ imply $3.087 < {}^{Ru}_{CeII}d_1 \le 3.097 \le {}^{Ru}_{CeI}d_1 <$ < 3.107 Å; similarly ${}^{Ru}_{RuI}d_1 = 2.645$ with $\Delta_{RuRu} = 0.006$ whence $2.639 < {}^{Ru}_{RuII}d_1 \le 2.645 \le {}^{Ru}_{RuI}d_1 < 2.651$ Å. The experimental range covers La $x \le 0.2$ and $x \ge 0.75$, both regions associated to $p_1 < 2.4\%$ (Fig. 3,*b*), low, yet not negligible probability of T_1 to the total population. Such a low presence does reflect on the reliability of estimations of the parameters deduced for T_1.

6. Conclusions

In this manuscript we have presented a statistical analysis showing that the $Ce_{1-x}La_xRu_2$ ternary system is essentially a mixture of two binaries: $CeRu_2$ and $LaRu_2$, with an extremely low content of the ternary $Ce_{0.5}La_{0.5}Ru_2$ configuration whose maximum concentration has been estimated $\le 3.15\%$ at the intermediate concentration of La $x =$ $= 0.5$. At the same time, the present study cannot rule out the presence of a distribution of mesoscopic phases in the $Ce_{1-x}La_xRu_2$ (i.e., a mesoscopic phase separation) characterized by different composition and functions, resulting due to susceptible electronic structure of the system (singularities in the band structure that could be manipulated easily by the substitution at the site A in the AB_2 structure, e.g., the Mg or the Rare Earth sites). Moreover from these data we recognize that while the ${}^{LaLa}T_2$ configuration exhibits a Bernoulli random distribution, the presence of a Ce atom affects both the ${}^{CeCe}T_0$ and ${}^{CeLa}T_1$ configuration distributions favoring the CeCe pair (Fig. 3,*a*,*b*) while keeping rare the ${}^{CeLa}T_1$ configuration with a single Ce ion.

This work is partially supported by the COMEPHS project.

1. S.S. Saxena, P. Agarwal, K. Ahilan, F.M. Grosche, R.K.W. Haselwimmer, M.J. Steiner, E. Pugh, I.R. Walker, S.R. Julian, P. Monthoux, G.G. Lonzarich, A. Huxley, I. Sheikin, D. Braithwaite, and J. Flouquet, *Nature* (*London*) **406**, 587 (2000).
2. J. Nagamatsu, N. Nakagawa, T. Muranaka, Y. Zenitani, and J. Akimitsu, *Nature* (*London*) **410**, 63 (2001).
3. C. Buzea and T. Yamashita, *Supercond. Sci. Technol*. **14**, R115 (2001).
4. C. Pfleiderer, M. Uhlarz, S.M. Hayden, R. Vollmer, H.V. Lohneysen, N.R. Bernhoeft, and G.G. Lonzarich, *Nature* (*London*) **412**, 58 (2001).
5. M. Imai, E. Abe, J. Ye, K. Nishida, T. Kimura, K. Honma, H. Abe, and H. Kitazawa, *Phys. Rev. Lett*. **87**, 077003 (2001).
6. M. Imai, K. Nishida, T. Kimura, and H. Abe, *Appl. Phys. Lett*. **80**, 1019 (2002).
7. H. Uchida, Y. Matsumura, H. Uchidab, and H. Kaneko, *J. Magn. Magn. Mater.* **239**, 540 (2002).
8. Q. Yao, J. Sun, Y. Zhang, and B. Jiang, *Acta Mater.* **54**, 3585 (2006).
9. D. Di Castro, *Ph.D. thesis*, Dipartimento di Fisica, Universita di Roma «La Sapienza» (2001).
10. B.T. Mattais, H. Suhl, and E. Corenzwit, *Phys. Rev. Lett*. **1**, 449 (1958).
11. D. Huxley, P. Dalmas de Rèotier, A. Yaouanc, D. Caplan, M. Couach, P. Lejay, P.C.M. Gubbens, and A.M. Mulders, *Phys. Rev*. **B54**, R9666 (1996).
12. A. Huxley, J.X. Boucherle, M. Bonnet, F. Bourdarot, I. Schustler, D. Caplan, E. Lelievre, N. Bernhoeft, P. Lejay, and B. Gillon, *J. Phys. Condens. Matter* **9**, 4185 (1997).
13. S.B. Roy and P. Chaddah, *Pramana — J. Physics* **53**, 659 (1999).
14. Ziyu Wu, N.L. Saini, S. Agrestini, D. Di Castro, A. Bianconi, A. Marcelli, M. Battisti, D. Gozzi, and G. Balducci, *J. Phys.: Condens. Matter* **12**, 6971 (2000).
15. N.L. Saini, S. Agrestini, D. Di Castro, Z. Wu, A. Bianconi, D. Gozzi, G. Balducci, and A. Marcelli, *J. Alloys Compounds* **317**, 542 (2001).
16. S. Agrestini, N.L. Saini, E. Amato, M. Filippi, D. Di Castro, G. Campi, P. Manfrinetti, and A. Bianconi, *J. Magn. Magn. Mater*. **272**, e139 (2004).
17. N.L. Saini, S. Agrestini, E. Amato, M. Filippi, D. Di Castro, A. Bianconi, P. Manfrinetti, A. Palenzola, and A. Marcelli, *Phys. Rev.* **B70**, 094509 (2004).
18. R.W.G. Wyckoff, *Crystal Structures*, Interscience Publishers, New York (1957), vol. I, p. 365.
19. A.L. Spek, *Acta Cryst*. **A46**, C-34 (1990).
20. T. Mihalisin, A. Harrus, S. Raaen, and R.D. Parks, *J. Appl. Phys*. **55**, 1966 (1984).
21. B.V. Robouch, A. Kisiel, and J. Konior, *J. Alloys Compounds* **339**, 1 (2002).
22. B.V. Robouch and A. Kisiel, *J. Alloys Compounds* **286**, 80 (1999).

23. B.V. Robouch, A. Kisiel, and J. Konior, *J. Alloys Compounds* **340**, 13 (2002).
24. B.V. Robouch, E.M. Sheregii, and A. Kisiel, *Fiz. Nizk. Temp.* **30**, 1225 (2004) [*Low Temp. Phys*. **30**, 921 (2004)]**.**
25. B.V. Robouch, E. Burattini, A. Kisiel, A.L. Suvorov, and A.G. Zaluzhnyi, *J. Alloys Compounds* **359**, 73 (2003).
26. *X-ray Absorption; Principles, Applications, Techniques of EXAFS, SEXAFS, XANES*, R. Prinz and D. Koningsberger (eds.), Wiley, New York (1988).
27. R.N. Shelton, A.C. Lawson, and K. Baberschke, *Solid State Commun*. **24**, 465 (1977).
28. L. Trıger, D. Arvanitis, K. Baberschke, H. Michaelis, U. Grimm, and E. Zschech, *Phys. Rev*. **B46**, 3283 (1992).